https://dx.doi.org/10.1016/j.conbuildmat.2022.128962

Kinetics-based fatigue damage investigation of asphalt mixture through residual strain analysis using indirect tensile fatigue test

Chenze Fang [a,b], Naisheng Guo [*,a], Zhen Leng [*,b], Jiwang Jiang [b], Hui Li [b], Guoyang Lu [b], Haopeng Wang [c]

[a] Department of Transportation Engineering, Dalian Maritime University, Dalian, Liaoning, 116026.

[b] Department of Civil and Environmental Engineering, The Hong Kong Polytechnic University, Kowloon, Hong Kong, 99907.

[c] Nottingham Transportation Engineering Centre, University of Nottingham, Nottingham, NG7 2RD, UK.

*Corresponding authors: 1. Naisheng Guo, naishengguo@126.com;

2. Zhen Leng, zhenleng@gmail.com.

E-mail addresses: fangchenze@126.com (C.Z. Fang); jiwang.jiang@polyu.edu.hk (J.W. Jiang);

huili94@zju.edu.cn (H. Li); guoyang.lu@polyu.edu.hk (G.Y. Lu);

haopeng.wang@nottingham.ac.uk (H.P. Wang).

Submitted to ***Construction and Building Materials.***

Abstract: Fatigue damage, one of the major distresses of asphalt pavement, has been found to have a phenomenological correlation with the accumulated residual strain (*RS*) of the asphalt mixture tested by stress-controlled fatigue test with excessive creep. However, it remains a challenge to quantitatively model such phenomenological correlation. This study aims to address this challenge by applying the kinetics theory to the indirect tensile fatigue test (ITFT) with excessive creep data of various asphalt mixtures. First, ITFTs of asphalt mixtures under different conditions were conducted to analyze the *RS* response. Then, the *RS* kinetics model was established based on the fast-constant rate kinetics model. Finally, two of the kinetics model parameters, the *RS* constant rate (k_c) and activation energy, were successfully applied to characterize the fatigue life (N_f) and the fatigue damage resistance of the asphalt mixture, respectively. It was found that the established *RS* kinetics model can accurately describe the development of the accumulated *RS* determined by ITFT. The k_c determined by ITFT is an effective indicator for the rate of the initial damage evolving to the failure threshold. The established k_c-based fatigue equation can be used to predict the N_f of the asphalt mixture tested by ITFT from k_c. The *RS* accumulation activation energy can effectively characterize the fatigue damage resistance of the asphalt mixture tested by ITFT.

Keywords: asphalt mixture; kinetics model; residual strain; fatigue damage

1 Introduction

Fatigue damage of asphalt mixture is one of the major distresses of asphalt pavement [1-4]. The fatigue damage of pavement with asphalt layers thicker than 200 mm can be modeled by the stress-controlled fatigue tests with excessive creep (such as ITFT), where the specimens will fail due to the coupled effects of excessive creep and fatigue damage. Although it is difficult to precisely separate both phenomena, many phenomenological approaches also are employed to investigate them successfully [5]. For example, the digital image correlation (DIC) method is usually used to characterize the crack propagation qualitatively. Jiang et al.'s [6-8] DIC results proved that the corresponding *RS* and fatigue cracking exhibit similar three-stage trends, and the fatigue damage evolution laws can be captured to a certain extent by identifying the development of the accumulated *RS*. It indicates that the fatigue damage of the asphalt mixture tested by the fatigue tests with excessive creep can be investigated from the *RS* perspective to a certain extent [9]. The *RS* and fatigue cracking of the asphalt mixture tested by the widely used stress-controlled fatigue tests will be produced simultaneously and coupled with each other. The fatigue cracking is difficult to be quantitatively characterized, so the *RS* can be a direct and promising parameter for approximating the degree of fatigue damage [5, 6].

Several empirical models were developed to predict the *RS* [10]. However, the prediction accuracy and efficiency of these models are highly dependent on the test condition due to their intrinsic empirical nature [11, 12]. To address the limitations of the empirical models, various rheological models were proposed, among which the modified *Burgers* model is capable of accurately characterizing the viscoelastic behavior of asphalt mixture [13-17]. Xu [16] established the modified *Burgers* model using a dashpot in tandem modified by an exponential function, based on which various *RS* models were developed to describe the *RS* under static repeated loading. Zhang et al. [17] proposed an *RS* model under dynamic repeated loading by transforming the dynamic load into the static load. Nevertheless, one shortcoming of the model is that it fails to capture the *RS* in the third stage. In order to characterize the three-stage *RS* under dynamic loading, Zhang et al. [18-20] developed an *RS* model by modifying the *Burgers* model with a quadratic function. It was concluded that the *RS* is mainly composed of nonlinear viscous strain and residual viscoelastic strain. Later, Fang et al. [21] applied the *RS* model proposed by Zhang et al. [18-20] to define the ratio of residual strain change (*RRSC*) for characterizing the resistance to the fatigue damage to a certain extent. Their results showed there exists a phenomenological correlation between the *RS* and fatigue damage of asphalt mixture tested by stress-controlled fatigue test with excessive creep. However, there have been very few studies that focus on quantitatively modelling such correlation [22, 23].

Fatigue damage of an asphalt mixture is a dynamic process with stages of different damage evolution rates, and N_f is a parameter which reflects the overall damage evolution rate of the mixture [5, 9, 21]. Accurately characterizing the varying-rate processes of the accumulated *RS* and damage is crucially important for reducing the damage evolution rate and extending the service life [24]. Previous studies [257] have shown that the kinetics theory can be applied to accurately characterize the evolution rate of a chemical or physical process. Herrington [26] proposed a kinetics-based viscosity model for asphalt binder by investigating the viscosity change law. Jin et al. [27] established an oxidation kinetics model of asphalt binder by investigating the changes of carbonyl area in binder's infrared spectrum. Luo et al. [28-30] successfully predicted the modulus of aged asphalt mixture by developing an aging kinetics model for asphalt pavement. Liu et al. [31, 32] developed a kinetics-based framework for measuring the rheological properties of aged asphalt binder. Recently, Luo et al. [33, 34] and Li et al. [35-37] applied kinetics theory to the healing in asphalt mixture and the cracking in asphalt binder, respectively.

Although kinetics theory has been applied in literature to evaluate various properties of viscoelastic materials, such as aging, healing and cracking, this theory has been seldomly applied to investigate the *RS* and damage of asphalt mixture. Correspondingly, this study aims to investigate the fatigue damage of asphalt mixture from the *RS* perspective by applying the kinetics theory. First, ITFTs were conducted on laboratory prepared asphalt mixture samples to analyze the *RS* response. Then, the *RS* kinetics model was established to determine the *RS* kinetics parameters, i.e, the *RS* constant rate and the activation energy. Finally, these two parameters were applied to investigate N_f, and the fatigue damage resistance, respectively.

2 Materials and Experimetnal Program

2.1 Materials and Specimen Preparation

Granite was selected as the aggregate to produce the stone mastic asphalt (SMA) mixture with the aggregate gradation shown in Table 1. SBS modified asphalt binder with a Superpave performance grade of 76-16 (PG76-16) and base asphalt binder with a penetration grade of 60/70 (Pen60/70) were selected to produce the SMA mixture specimens with the target air void content of 4% and the binder content of 6%. The basic properties of the selected binders are shown in Table 2. In order to simulate the aging condition, asphalt mixture was aged in the oven at 135°C for 4 hours and then fabricated into cylindrical specimens. The cylindrical specimens with the size of 150 mm in height and 100 mm in diameter were compacted using a gyratory compactor. The top and bottom layers with a height of 15mm were cut to obtain the cylindrical specimens with the size of 100 mm in diameter and 40 mm in thickness, as shown in Fig. 1.

Table 1 Aggregate gradation

Composition	Bulk specific gravity (g/cm^3)	Sieve size (mm)	Percentage (%)
Coarse aggregates	2.642	14-10	3.5
	2.663	10-5	59.5
	2.709	5-2.36	9.0
Fine aggregates	2.649	2.36-0.075	16.5
Mineral filler	2.661	<0.075	9.5
Hydrated lime	2.587		2.0

Table 2 Technical properties of asphalt binders

Indices	PG76-16	Pen60/70
Penetration (25℃, 100 g, 5 s) (0.1 mm)	46	64.5
Softening point (°C)	93	50
Viscosity (135°C) (m Pa·s)	2450	477.5

（a）Specimen （b）Measuring horizontal tensile strain

Fig. 1. Indirect tensile fatigue test

2.2 Experimental Program

The stress-controlled ITFT was conducted in this study to simulate the fatigue damage behavior of asphalt mixture, because of advantages, such as simple specimen preparation and high repeatability [8]. Therefore, the ITFT was carried out to verify the feasibility of investigating the fatigue damage asphalt mixture based on the residual strain (*RS*) kinetics characterization.

To investigate the effects of temperature, loading frequency, binder type and aging on the fatigue damage of asphalt mixture by applying the kinetics theory, the ITFTs were carried out according to the test conditions summarized in Table 3. The load ratio was 0.3 and the half-sine load pulse was repeatedly applied by an UTM-30 machine. The applied force amplitude was equal to the product of the load ratio and the maximum force measured at the loading rate of 50mm/min [8].

Table 3 ITFT conditions

Test number	Asphalt binder type	Temperature (℃)	Frequency (Hz)	Aged/Unaged	N_f
1	PG76	25	10	Unaged	5173
2	PG76	15	10	Unaged	8209
3	PG76	5	10	Unaged	12514
4	PG76	15	5	Unaged	3389
5	PG76	15	2	Unaged	2157
6	PG76	25	10	Aged	10994
7	PG76	15	10	Aged	35137
8	PG76	5	10	Aged	97541
9	60/70	25	10	Unaged	1691
10	60/70	15	10	Unaged	2907
11	60/70	5	10	Unaged	3133

There is a non-negligible error between the horizontal tensile strain calculated by the vertical displacement data and the true horizontal tensile strain. Therefore, epoxy glue was used to glue two steel sheets on both sides of the cylindrical specimen, and the horizontal tensile strain (ε_t) was continually monitored by the two LVDTs installed in the holes of the steel sheets. It can be observed from Fig. 2, the ε_t curve exhibits a rising cyclic trend, and the strain at each trough is defined as the *RS*. The tested specimens will fail due to the coupled effects of excessive creep and fatigue damage. The corresponding *RS* and fatigue cracking that are coupled with each other will be produced simultaneously. Compared with the fatigue cracking difficult to be quantitatively characterized, the *RS* can be a direct and promising parameter for approximating the degree of fatigue damage to a certain extent [5, 6].

According to all related conducted researches [5, 9, 21], the ratio of residual strain change (*RRSC*) represented as Eq. (1) can indicate the resistance to the fatigue damage of the asphalt mixture tested by the stress-controlled fatigue tests with excessive creep to a certain extent, and the damage evolution rate can be positively correlated with the *RRSC*. Fig. 3 illustrates that the *RRSC*-*N* curve is composed of three stages. The intersection point F of the tangents of the second and third stages is the failure point where the damage reaches the failure threshold and the material structure becomes seriously unstable. The loading cycle number corresponding to the point F is recorded as the fatigue life (N_f).

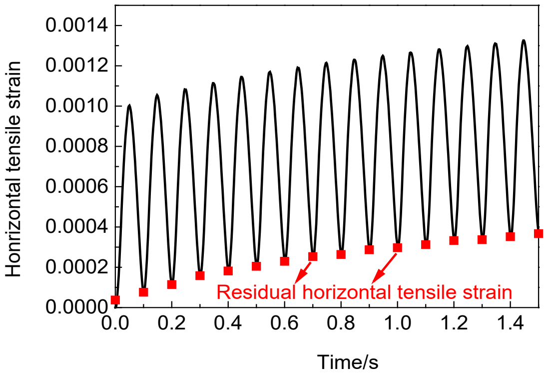

Fig. 2. Horizontal tensile strain curve

$$RRSC = \frac{RS_{N+1} - RS_N}{RS_N} \tag{1}$$

where RS_N is the residual strain of the loading cycle *N*.

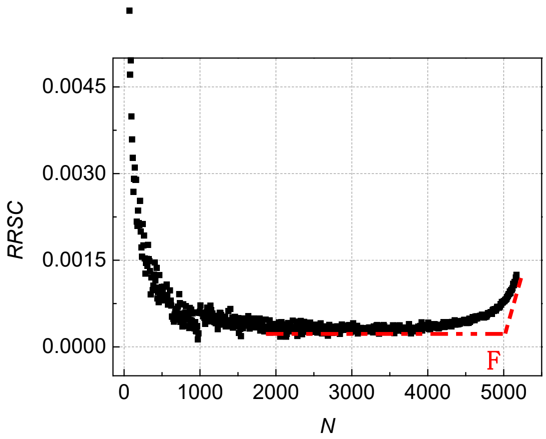

Fig. 3. *RRSC-N* curve

3 Residual Strain Response Analysis

3.1 Residual Strain Empirical Model

Zhang et al. [14, 18-20] developed the *RS* empirical model, and the derivation process can be elaborated in Eqs. (2)-(11). This empirical model has been used to describe the overall *RS* trend of the asphalt mixture tested by ITFT. Because the corresponding *RS* and fatigue cracking that are coupled with each other will be produced simultaneously. This *RS* empirical model can reflect the process of fatigue damage to a certain extent. Moreover, this model can be widely used in the field of road engineering and indoor tests because of its simple form and derivations.

The strain of a visoelastic asphalt mixture mainly includes three components, namely the elastic strain (ε_{e}), the viscoelastic strain (ε_{ve}) and the nonlinear viscous strain (ε_{nlv}) [14, 18-21]. After the applied load is removed, the ε_{nlv} and partial ε_{ve} are unrecoverable, while the ε_{e} can be fully recovered. In this paper, the sum of the unrecovered viscoelastic strain (ε_{rve}) and ε_{nlv} is defined as the residual strain (*RS*) that can be approximately recorded as the strain corresponding to the red dots as shown in Fig 2 [5, 9, 21], as shown in Eq. (2).

$$\varepsilon_{r,N} = \varepsilon_{nlv} + \varepsilon_{rve} \tag{2}$$

where the $\varepsilon_{r,\,N}$ is the accumulated *RS*.

Traditional *Burgers* model with the simple form and derivations has been widely used in the field of road engineering. Its defects can also be addressed to a certain extent by the modified *Burgers* model combined with the modified tandem dashpot (η_{v}) and the *Van Der Poel* model. Therefore, Zhang et al. [14, 18-20] developed the *RS* empirical model based on the modified *Burgers* model, which can describe the *RS* accumulation process. In their works, the residual viscoelastic strain can be determined by the *Van Der Poel* model with the creep compliance ($J(t)$) calculated by Eq. (3). And the nonlinear viscous flow strain can be determined by the η_v with the viscous coefficient calculated by Eq. (4).

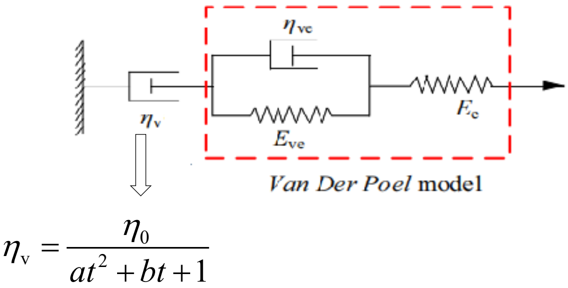

Fig. 4 Modified *Burgers* model

$$J(t) = \frac{1}{E_e} + \frac{1}{E_{ve}}(1 - e^{-E_{ve} t/\eta_{ve}}) \tag{3}$$

where E_e and E_{ve} are the elastic moduli of the tandem and parallel springs; η_{ve} is the viscous coefficient of the parallel dashpot.

$$\eta_v = \frac{\eta_0}{at^2 + bt + 1} \tag{4}$$

where η_0 is the initial viscous coefficient of η_v; a and b are constants.

Boltzmann principle can be applied to determine the dynamic strain responses of the viscoelastic material under non-constant load, as expressed in Eq. (5). *Van Der Poel* model is a linear viscoelastic body, and *Boltzmann* principle can be applied to derive the residual viscoelastic strain under half-sine pulse load [14, 18-20].

$$\varepsilon = \int_0^t J(t - \tau) \frac{d\sigma}{d\tau} d\tau \tag{5}$$

where ε and σ are the viscoelastic strain and stress of the viscoelastic material, respectively; and τ is the arbitrary time between 0 and t.

At the end of loading cycle N, the residual viscoelastic strain caused by the ith pulse load ($\varepsilon_{rve,i}$) can be derived as Eq. (6) [14, 18-20].

$$
\begin{aligned}
\varepsilon_{\mathrm{rve},i} &= \int_0^T \mathrm{J}\left[NT-(i-1)T-\tau\right]\frac{\mathrm{d}\sigma(\tau)}{\mathrm{d}\tau}\mathrm{d}\tau \\
&= \int_0^T \left\{ \frac{1}{E_e} + \frac{1}{E_{ve}}(1\text{-}e^{-\frac{E_{ve}[NT-(i-1)T-\tau]}{\eta_{ve}}}) \right\} \frac{\sigma_0 \pi}{T}\cos\frac{\pi\tau}{T}\mathrm{d}\tau \\
&= \frac{\pi\sigma_0 T(1+e^{E_{ve}T/\eta_{ve}})}{\eta_{ve}(\frac{E_{ve}^{\ 2}}{\eta_{ve}^{\ 2}}T^2+\pi^2)} e^{-\frac{E_{ve}}{\eta_{ve}}[N-(i-1)]T}
\end{aligned} \tag{6}
$$

where T is the loading period; σ_0 is the loading amplitude. The loading time from loading cycle i to the end of loading cycle N is equal to NT-(i-1)T. Therefore, N was involved when calculating $\varepsilon_{\mathrm{rve},i}$ [14, 18-20].

After N loading cycles, the accumulated residual viscoelastic strain ($\varepsilon_{\mathrm{rve},N}$) is expressed as follows [14, 18-20].

$$
\varepsilon_{\mathrm{rve},N} = \sum_{i=1}^{N} \varepsilon_{\mathrm{rve},i} = \lambda(1-e^{-\kappa N}) \tag{7}
$$

where $\lambda = \dfrac{\pi T(1+e^{E_{\mathrm{ve}}T/\eta_{ve}})e^{-E_{\mathrm{ve}}T/\eta_{ve}}\sigma_0}{\eta_{ve}(\frac{E_{\mathrm{ve}}^{\ 2}}{\eta_{ve}^{\ 2}}T^2+\pi^2)(1-e^{-E_{\mathrm{ve}}T/\eta_{ve}})}; \kappa = \dfrac{E_{ve}}{\eta_{ve}}T.$

The $\varepsilon_{\mathrm{nlv}}$ of the viscoelastic material under half-sine pulse load can be determined by Eq. (8) [14, 18-20].

$$
\varepsilon_{\mathrm{nlv}} = \int_0^t \frac{\sigma}{\eta_{\mathrm{v}}(\tau)}\mathrm{d}\tau \tag{8}
$$

At the end of loading cycle N, the $\varepsilon_{\mathrm{nlv}}$ caused by the ith pulse load ($\varepsilon_{\mathrm{nlv},i}$) can be derived as Eq. (9) [14, 18-20].

$$
\begin{aligned}
\varepsilon_{\mathrm{nlv},i} &= \int_0^T \frac{\sigma(\tau)}{\eta_{\mathrm{v},i}(\tau)}\mathrm{d}\tau = \frac{\sigma_0}{\eta_0}\int_0^T \sin\frac{\pi\tau}{T}\left\{a[(i-1)T+\tau]^2 + b[(i-1)T+\tau]+1\right\}\mathrm{d}\tau \\
&= \frac{2a\sigma_0 T^3}{\pi\eta_0}(i-1)^2 + \frac{2b\sigma_0 T^2 + 2a\sigma_0 T^3}{\pi\eta_0}(i-1) + \frac{\sigma_0}{\pi\eta_0}(2T + bT^2 + aT^3 - \frac{4aT^3}{\pi^2})
\end{aligned} \tag{9}
$$

After N loading cycles, the accumulated nonlinear viscous strain ($\varepsilon_{\mathrm{nlv},N}$) is expressed as follows [14, 18-20].

$$
\varepsilon_{\mathrm{nlv},N} = \sum_{i=1}^{N} \varepsilon_{\mathrm{rvf},i} = \alpha N^3 + \beta N^2 + \gamma N \tag{10}
$$

where $\alpha = \frac{2aT^{3}\sigma_0}{3\eta_0\pi}; \beta = \frac{bT^2\sigma_0}{\eta_0\pi}; \gamma = \sigma_0 \frac{6\pi^2 T + \pi^2 aT^{3} - 12aT^{3}}{3\eta_0\pi^3}$.

Then, the *RS* empirical model can be established as Eq. (11). More details about the *RS* empirical model can be found in [14, 18-20].

$$\varepsilon_{\mathrm{r},N} = \alpha N^3 + \beta N^2 + \gamma N + \lambda(1 - e^{-\kappa N}) \tag{11}$$

The *RS*-*N* curves were fitted by Eq. (11) and the fitting result is shown in Fig.5 and Table 4. Tests 2, 4 and 5 with different loading frequencies were under the same material type and temperature. The E_{ve}, η_{ve}, η_0, obtained from test 2 can accurately describe the *RS* in tests 4 and 5 only when the a and b are different, which indicates the developed model is an empirical model and can describe the *RS* mathematically.

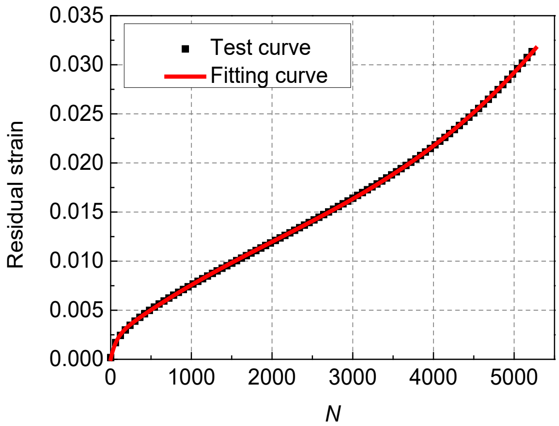

Fig. 5. Fitting result of *RS* empirical model

Table 4 Fitting results of *RS* empirical model

Test number	E_{ve} (MPa)	η_{ve} (MPa·s)	a ($\times 10^{-8}$ s^{-2})	b (s^{-1})	η_0 (MPa·s)	R^2
1	81.36955	538.32068	822.549	-0.001660001	2693.90203	0.99841
2	251.51738	3838.07685	200.726	-0.000761068	18132.64039	0.99832
3	700.06809	57500.20141	158.959	-0.000440258	111705.4454	0.99946
4	251.51738	3838.07685	558.165	-0.001030001	18132.64039	0.98838
5	251.51738	3838.07685	142.258	-0.000245115	18132.64039	0.99745
6	149.42999	2320.27005	1.65667	-0.000689779	12386.06813	0.99979
7	194.24146	5686.33347	19.8715	-0.000246996	59621.08029	0.99984
8	371.14205	49361.98726	2.47822	-0.000086441	325834.6818	0.99986
9	63.22769	159.07404	8536.31	-0.005100002	552.86702	0.9999
10	173.64888	427.16173	3207.08	-0.002800012	2240.22627	0.99994
11	1295.39002	2210.31873	3298.01	-0.003470001	10481.70196	0.99971

3.2 Residual Strain Response Analysis

The overall damage evolution rate of asphalt mixture can be reflected by N_f. Fig. 6 illustrates the *RS* response under different conditions. N_f exhibits a decreasing trend with the increase of the *RS* rate. From Fig. 6 (a) and (b), it can be seen that the *RS* response is highly dependent on temperature and loading frequency [38-41]. At high loading frequency and low temperature, the asphalt mixture exhibits slower *RS* rate and longer N_f. This is because the asphalt mixture behaves in a more elastic way under such conditions [42-44]. Thus, it exhibits greater capacity in supporting more cyclic loading without flow [1-4]. Consequently, the brittle fracture occurs, as shown in Fig. 7 (a): the cracks are thin and un-ramified. In contrast, at low frequency and high temperature, the asphalt mixture exhibits larger *RS* rate and shorter N_f. This is because the viscoelastic material behaves in a more viscous way of being susceptible to accumulating the *RS*. Therefore, the ductile fracture occurs, as shown in Fig. 7 (b): the cracks are wide and ramified [1-4].

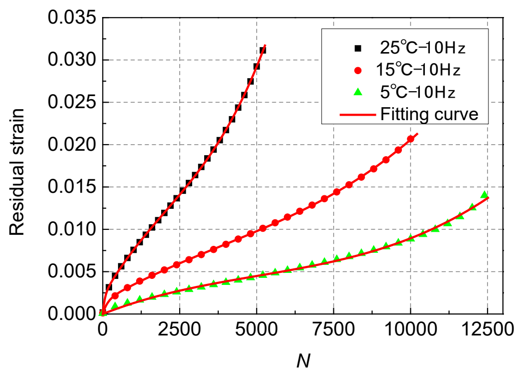

(a) (PG76-16)-25/15/5℃- 10Hz-Unaged

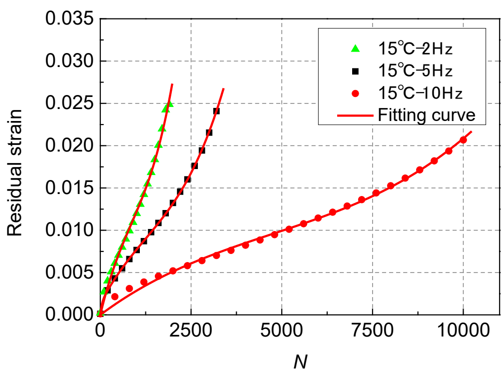

(b) (PG76-16)-15℃- 10/5/2Hz-Unaged

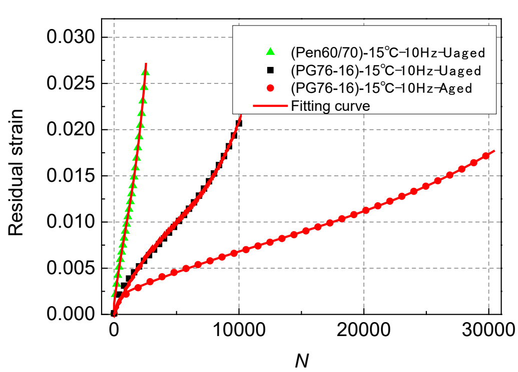

(c) (Pen60/70)/(PG76-16)-15℃- 10Hz-Unaged/Aged

Fig. 6. Residual strain results

(a) Brittle fracture at low temperature and high frequency **(b)** Ductile fracture at high temperature and low frequency

Fig. 7. Brittle and ductile fracture damages

As illustrated in Fig. 6 (c), compared with the asphalt mixture with base binder (Pen60/70), the SBS modified asphalt mixture exhibits slower *RS* rate and longer N_f. This is because the SBS modifiers form the complex polymer network in asphalt binder structure. The network leads to the more elastic mechanical response, which retards the appearance of strain hardening [1-4]. Accordingly, the *RS* accumulation are retarded. Similarly, aging can increase the content of asphaltenes with larger molecular weight in asphalt binder, meaning the weaker asphaltenes/maltenes relationship. Then the asphalt binder structure becomes stiffer leading to the more elastic mechanical response. Consequently, the aged asphalt mixture is less susceptible to accumulating the *RS* and can be resistant to more loading cycles than the unaged one [1-4].

As discussed above, the faster *RS* enters the third stage, the faster the fatigue damage evolves to the threshold. There exists a phenomenological correlation between the *RS* rate and the N_f of the asphalt mixture tested by ITFT. This is because the *RS* and fatigue damage will be produced simultaneously and coupled with each other in the corresponding cyclic loading process, where the specimens will fail due to the coupled effects of excessive creep and fatigue damage. The fatigue damage evolution laws can be captured to a certain extent by identifying the development of the accumulated *RS* [6-9].

Kinetics theory can be applied to accurately characterize the evolution rate of a chemical or physical process. In section 3, the *RS* empirical model inherited from previous studies [14, 18-20] has been used to describe the overall *RS* trend. The following chapters will verify the feasibility of modeling the phenomenological correlation between the *RS* and fatigue damage using the kinetics theory.

4 Kinetics-based Fatigue Damage Investigation of Asphalt mixture

4.1 Kinetics Characterization of Residual Strain

In kinetics theory, the chemical or physical process reaching its equilibrium can be quantified by the representative rate constant (k). In addition, the required minimum input energy ensuring the process to proceed is called activation energy (E_a), which indicates the reaction difficulty degree and depends on the material properties and process conditions [25, 26]. The key procedure of the kinetics approach is to establish the kinetics model and obtain the kinetics parameters (the k and the E_a). The commonly used *Arrhenius* kinetics equation is shown in Eq. (12), which can accurately determine the relationship between k and E_a [27, 28].

$$k = Ae^{\frac{-E_a}{RT}} \tag{12}$$

where A is the exponential factor; R is the gas constant; and T is the absolute temperature.

Eq. (13) presents the commonly used kinetics model of viscoelastic materials, which can accurately simulate the chemical or physical processes with two stages, namely the fast stage and the constant stage, such as the change laws of carbonyl, modulus and viscosity of asphalt binder during the aging process [27-30]. Taking the natural logarithm of the *Arrhenius* kinetics equation, Eq. (12) can be converted to Eq. (14). The rate constants at different temperatures are fitted by Eq. (14) for determining the E_a equal to the fitted slope.

$$y = y_{\text{initial}} + (y_0 - y_{\text{initial}})(1 - e^{-k_f x}) + k_c x \tag{13}$$

$$\ln k = \ln A - \frac{E_a}{RT} \tag{14}$$

where y is the dependent variable; y_{initial} is the initial value of y; y_0 is the intercept of the constant rate line of growth of y versus x; k_f is the fast rate; x is the independent variable; k_c is the constant rate; and k *is* the representative rate.

As illustrated in Fig. 8, the overall *RS* accumulation trend exhibits three stages, namely the fast rate stage, the constant rate stage and the acceleration stage, among which the serious structure instability occurs at the acceleration stage leading to the evolution with high discreteness and uncertainty. Additionally, the damage evolution of the third stage is the evolution result of the first two stages, and accounts for a small proportion. Consequently, establishing the kinetics-based model to predict the *RS* in the first two stages is of great significance for describing the overall rate process of the accumulated *RS* [5, 9, 21].

The *RS* and *N* correspond to the dependent variable of y and the independent variable of x in Eq. (13), respectively. The initial *RS* value can be regarded as 0, that was, y_{initial}=0. Substituting y_{initial}=0 into Eq. (13), the *RS* kinetics model was established as shown in Eq. (15). The fast rate stage and constant rate stage of the *RS* accumulation process can be described by the k_f and k_c, respectively. Given that the proportion of the fast rate stage corresponding to the k_f is small, the k_c is selected as the representative rate in Eq. (14) for quantifying the overall accumulation rate of the *RS* and the required minimum input energy ensuring the process of *RS* accumulation to proceed. The *RS* increases steadily in the constant rate stage with the main proportion and the *RS* rate steadily approaches a constant value, which means the k_c can be approximately obtained by loading to a certain cycle before the end of the constant rate stage and this cycle can theoretically be much less than N_f. Eq. (15) is used to fit the test *RS* curve in the fast and the constant rate stages, and the fitting results are shown in Fig. 8 and Table 5. As observed, the fitting curve shows good agreement with the test curve, which means the developed kinetics-based model is able to model the overall trend of the *RS* curve.

$$\begin{aligned}\varepsilon_{\mathrm{r}} &= \varepsilon_{\mathrm{r},0}(1-e^{-k_{\mathrm{f}}N}) + k_{\mathrm{c}}N \\ &= \varepsilon_{\mathrm{r},0}\left(1-e^{\left(-A_{\mathrm{f}}e^{\frac{-E_{a,\mathrm{f}}}{RT}}\right)N}\right) + \left(A_c e^{\frac{-E_{a,\mathrm{c}}}{RT}}\right)N\end{aligned} \tag{15}$$

where ε_r is the residual strain; k_f, A_f and $E_{a,f}$ are the fast rate, exponential factor and activation energy of the *RS* in the fast rate stage, respectively; k_c, A_c and $E_{a,c}$ are the constant rate, exponential factor and activation energy of the *RS* in the constant rate stage; $\varepsilon_{r,0}$ is the intercept of the constant rate stage.

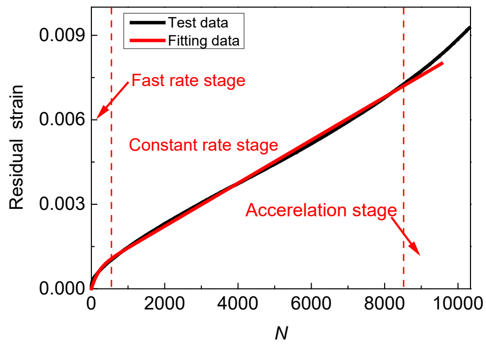

Fig. 8. *RS* kinetics model fitting

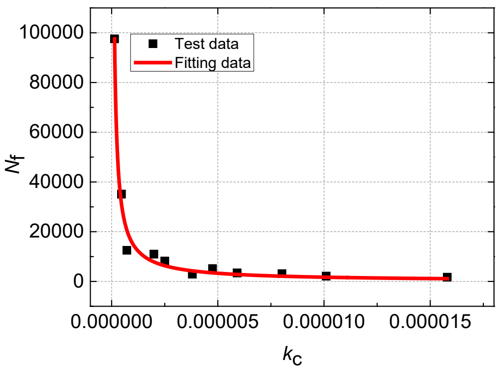

Fig. 9. Fitting results of N_f-k_c curve

Fig. 9 presents the N_f-k_c curve. As presented, the k_c (in the stable damage evolution process) exhibits a good correlation with the N_f. The corresponding *RS* and fatigue cracking will be produced simultaneously and coupled with each other. According to the kinetics theory, *RS* rate can be used to determine the material property of activation energy representing the minimum energy required for the development of the accumulated *RS* and fatigue damage. Therefore, the remaining chapters will verify the feasibility of investigating fatigue damage using the kinetics theory.

Table 5 Fitting results of *RS* kinetics model

Test number	N_f	k_c	k_f	R^2
1	5173	4.75E-06	0.01169691	0.9014
2	8209	2.50E-06	0.00421913	0.9214
3	12514	7.17E-07	0.00273325	0.9612
4	3389	5.91E-06	0.01814621	0.9712
5	2157	1.01E-05	0.02360068	0.9423
6	10994	1.99E-06	0.00402244	0.9111
7	35137	4.65E-07	0.00250097	0.9321
8	97541	1.39E-07	0.00060709	0.9345
9	1691	1.58E-05	0.04096532	0.9364
10	2907	8.02E-06	0.01648633	0.9145
11	3133	3.80E-06	0.01831483	0.9712

4.2 Fatigue Life Investigation Base on Residual Strain Constant Rate

Fang et al. [5, 21] and Sun et al. [9] quantified the *RS* rate by defining the *RRSC*, and determined the phenomenological correlation between the *RS* and fatigue damage of asphalt mixture tested by the fatigue tests with excessive creep using the *RRSC*. Their results showed the potential of the *RRSC* as an effective parameter for indicating the resistance of asphalt mixture under stress-controlled mode to the fatigue damage, and the resistance is negatively correlated with the *RRSC*. In this paper, the fatigue damage of asphalt mixture is defined by modulus degradation to analyze the process of fatigue damage, as shown in Eq. (16).

$$D = \frac{S_0 - S_N}{S_0} \tag{16}$$

where D is damage variable; S_0 is initial stiffness modulus; and S_N is stiffness modulus of the loading cycle N [5]. Fig.10 presents the damage evolution curve of asphalt mixture [5, 9, 21]. It can be seen that *RS* rapidly increases at the fast rate of k_f in the first stage for a short period, and then the *RS* rate becomes slow leading to rapidly decreasing *RRSC*. Meanwhile, D rapidly reaches a higher level but the damage evolution rate (D_s) gradually decreases. The main damage stage is the second stage, where *RS* increases at the relatively constant rate of k_c. The corresponding *RRSC* steadily approaches a stable value, indicating stable resistance to damage accumulation. Consequently, D_s tends to stabilize and D increases slowly. Eventually, *RS* rapidly increases in a short time leading to the sharply increasing *RRSC*, and the material structure reaches N_f when D evolves to the failure threshold. The faster *RS* enters the third stage, the faster the fatigue failure occurs.

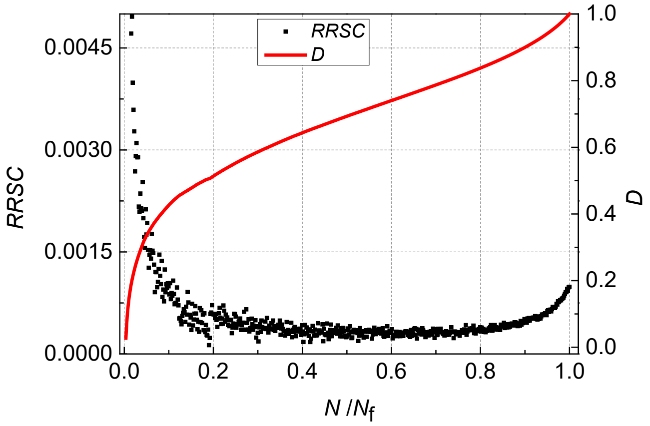

Fig. 10. Damage evolution analysis curve

As discussed above, N_f and *RS* rate exhibit a close correlation. The faster *RS* enters the third stage, the faster the initial damage ($D_{initial}$) evolves to the threshold ($D_{threshold}$) leading to shorter N_f, as Eq. (17) and Eq. (18) indicate. Theoretically, $D_{initial}$ and $D_{threshold}$ can be regarded as 0 and 1, respectively. N_f and damage evolution rate (D_s) are negatively correlated, as shown in Eq. (18). The main damage evolution stage is the second stage (constant rate stage) where *RS* steadily increases at the constant rate of k_c and D evolves at the stable rate of D_s, which means D_s can be determined from k_c. Therefore, k_c was used to establish the fatigue equation in the simple power function form. The fitting results are shown in Eq. (19) and Fig. 9. It can be seen that R^2 is more than 0.98. In order to verify the validity of the fatigue equation, the ITFTs were carried out according to the test conditions summarized in Table 6, and the measured k_c were substituted into Eq. (19) to predict the N_f results. As observed in Table 6, the relative errors between the measured N_f and predicted N_f at different temperatures were 7.4% and 12.5%, respectively, indicating the fatigue equation can quantify the relationship between k_c and N_f with reasonable accuracy.

Table 6 Comparison results between predicted N_f and measured N_f.

Asphalt binder type	Temperature (℃)	Frequency (Hz)	Aged / Unaged	k_c	Measured N_f	Predicted N_f	Relative error (%)
PG76	20	10	Unaged	2.61E-06	6512	6971	7
PG76	10	10	Unaged	2.11E-06	9210	8348	9.3

$$D(N) = \int_0^N D_s(N)dN \tag{17}$$

$$N_f = f(D_s, D_{initial}, D_{threshold}) = f(D_s, 0, 1) \tag{18}$$

$$N_f = 0.13763\ (k_c)^{-0.84269},\ R^2 = 0.9859 \tag{19}$$

4.3 Fatigue Damage Resistance Investigation Based on Residual Strain Accumulation Activation Energy

E_a represents the minimum energy required for a specific process. Therefore, it is negatively correlated with the reaction difficulty degree [25, 26]. Eq. (15) was used to fit k_c at different temperatures to obtain the E_a corresponding to k_c ($E_{a,c}$). The $E_{a,c}$ results are shown in Fig. 11 and Table 7. As presented, the ascending ranking of the tested mixtures in terms of $E_{a,c}$ is Pen60/70 (49.2185kJ·mol^{-1}), unaged PG76-16 (63.7394kJ·mol^{-1}) and aged PG76-16 (91.6217kJ·mol^{-1}), which is consistent with the ranking in *RS* rate and N_f as illustrated in Fig. 6(c). Therefore, it can be reasonably inferred that the $E_{a,c}$ can be used to characterize the difficulty degree of *RS* accumulation and predict the damage resistance. A larger $E_{a,c}$ indicates more energy is required to accumulate *RS*, and the mixture is less susceptible to *RS* accumulation, leading to stronger damage resistance.

Table 7 $E_{a,c}$ results

Test condition number	Test condition	$E_{a,c}$ (kJ • mol^{-1})
1	(Pen60/70)-10Hz-Uaged	49.2185
2	(PG76-16)-10Hz-Unaged	63.7394
3	(PG76-16)-10Hz-Aged	91.6217

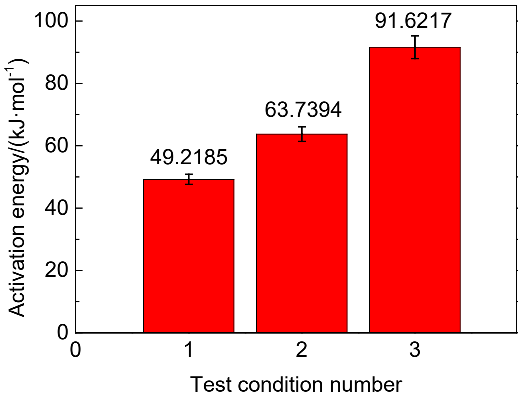

Fig. 11. $E_{a,c}$ results

5 Conclusions and Recommendations

In this study, the ITFT was conducted to develop the *RS* kinetics model, and the kinetics theory was applied to investigate the fatigue damage of asphalt mixtures. The following points summarize the major findings of this study:

• The *RS* rate of the asphalt mixture tested by ITFT is negatively correlated with the fatigue life (N_f). The established *RS* kinetics model can describe the whole corresponding *RS* accumulation process with high accuracy.

• The *RS* constant rate (k_c) of the asphalt mixture tested by ITFT is used to represent the rate of the initial damage evolving to the failure threshold. The established k_c-based fatigue equation can be used to predict the corresponding N_f from k_c.

• The *RS* accumulation activation energy of the asphalt mixture tested by ITFT measures the difficulty degree of *RS* accumulation. It can be used to characterize the corresponding damage resistance of an asphalt mixture.

• Note that the above conclusions may work for the stress-controlled ITFT, where creep and fatigue cracking will be produced simultaneously and coupled with each other, but not for tests with less of this excessive creep phenomenon, such as fatigue tests with centered sinusoidal signals, with zero residual strain, and that produce fatigue failure.

The outcomes of this study prove that the kinetics theory can be used as a powerful tool to investigate the fatigue damage evolution of the asphalt mixture tested by ITFT from the perspective of *RS* accumulation. Theoretically, these conclusions may work for other stress-controlled fatigue tests, where the specimens will fail due to the coupled effects of excessive creep and fatigue damage. However, more research is still needed to evaluate the effects of other test variables, such as material types, loading conditions and test types on the performance of the models developed in this study and verify their general applicability. Furthermore, the obtained results should be correlated with the field performance of asphalt pavement, and integrated into pavement design to ensure that the same level of correspondence based on the laboratory test data remains valid for pavement field performance.

Acknowledgments

This study was funded by the National Natural Science Funding of China under Grant No. 51308084, the Natural Science Foundation Project of Liaoning No. 2018010659-301 and the Special Subsidized Project of Basic Scientific Research Business Fees in Central Universities under Grant No. 3132017029.

References

[1] F. Moreno-Navarro, M.C. Rubio-Gámez, A review of fatigue damage in bituminous mixtures: Understanding the phenomenon from a new perspective, Constr. Build. Mater. 113 (2016) 927-938.

[2] F. Moreno, M. Sol-Sanchez, F. Moreno-Navarro, et al., Fatigue behavior of macro fiber reinforced gap graded asphalt mixtures, Mater. Struct. 53 (4) (2020)

[3] F. Moreno-Navarro, M.C. Rubio-Gάmez, UGR-FACT test for the study of fatigue cracking in bituminous mixes, Constr. Build. Mater. 43 (2013) 184-190.

[4] F.Moreno-Navarro, M.C. Rubio-Gάmez, Mean damage parameter for the characterization of fatigue cracking behavior in bituminous mixes, Mater. Des. 54 (2014) 748-754.

[5] C.Z. Fang, Research on damage evolution and fatigue life prediction of asphalt mixture, Shenyang Jianzhu University. Shenyang, 2019. (in Chinese)

[6] J.W. Jiang, Investigation of the fatigue property and internal structure of asphalt mixtures based on multiscale methods, Southeast University. Nanjing, 2019.(in Chinese)

[7] J.W. Jiang, F.J. Ni, Q. Dong, et al., Fatigue damage model of stone matrix asphalt with polymer modified binder based on tensile strain evolution and residual strength degradation using digital image correlation methods, Measurement. 123 (2018) 30-38.

[8] J.W. Jiang, F.J. Ni, Evaluation of fatigue property of asphalt mixtures based on digital image correlation method, Journal of Southeast University (English Edition). 33 (2) (2017) 216-223.

[9] Y.Z. Sun, C.Z. Fang, J.C. Wang, et al., Method of fatigue-life prediction for an asphalt mixture based on the plateau value of permanent deformation ratio, Materials. 11 (5) (2018) 1-16.

[10] P. Ayar, F. Moreno-Navarro, M. Sol-Sάnchez, et al., Exploring the recovery of fatigue damage in bituminous mixtures: the role of rest periods, Mater. Des. 51 (25) (2018)

[11] J.P. Zhang, X.M. Huang, T. Ma, Study on damage-creep characteristics and model of asphalt mixture, Chin. J. Geotech. Eng. 12 (2008) 1867-1871. (in Chinese)

[12] S. Hussan, M. A. Kamal, I. Hafeez, et al., Evaluation and modelling of permanent deformation behavior of asphalt mixtures using dynamic creep test in uniaxial model, Int. J. Pavement Eng. 20 (9) (2019) 1026-1043.

[13] I.L. Al-Qadi, P.J. Yoo, M.A. Elseifi, et al., Creep behavior of hot-mix asphalt due to heavy vehicular tire loading, J. Eng. Mech. 135 (1) (2009) 1265-1273.

[14] J.P. Zhang, X.M. Huang, H. Li, Permanent deformation of asphalt mixture under repeated load, Chin. J. Southeast. Univ. (Nat. Sci. Ed). 38 (3) (2008) 511-515. (in Chinese)

[15] R. A. Schapery, Nonlinear viscoelastic and viscoplastic constitutive equations with growing damage, Int. J. Fract. 97 (1999) 33-66.

[16] S. F. Xu, Prediction and control of rutting in asphalt pavements, Tongji University, Shanghai, China,1991. (in Chinese)

[17] Y.Q. Zhang, X.M. Huang, Viscoelastic mechanical model of permanent deformation of asphalt mixtures under repeated load, Journal of Highway and Transportation Research and Development. 25 (4) (2008) 1-6. (in Chinese)

[18] J.P. Zhang, X.M. Huang, Viscoelastic model for asphalt mixture under repeated haversine load, J. Southeast. Univ. (English. Ed). 25 (4) (2009) 523-526.

[19] J.P. Zhang, Z.P. Fan, K. Fang, et al., Development and validation of nonlinear viscoelastic damage (NLVED) model for three-stage permanent deformation of asphalt concrete, Constr. Build. Mater. 102 (2016) 384-392.

[20] J.Z. Pei, Z.P. Fan, J.P. Zhang, et al., Nonlinear viscoelastic model for asphalt mixture subjected to repeated loading, Road. Mater. Pavement. 17 (4) (2016) 892-905.

[21] C.Z. Fang, N.S Guo, ZP. You, Y.Q. Tan, Investigating fatigue life prediction of rubber asphalt mixture based on damage evolution using residual strain analysis approach, Constr. Build. Mater. 257 (2020) 119476.

[22] H. Di Benedetto, C. de La Roche, H. Baaj, A. Pronk, R. Lundstron, Fatigue of bituminous mixtures: different approaches and RILEM group contribution, in: Proceedings of the 6th International RILEM Symposium, Zurich, Swiss, 2003.

[23] I. Artamendi, H. Khalid, Characterization of fatigue damage for paving asphaltic materials, Fatigue Fract. Eng. Mater. Struct. 28 (2005) 1113-1118.

[24] A.A. Rose, I.R. Lenz, C.T. Than, C.J. Glover, Investigation of the effects of recycled engine oil bottoms on asphalt field performance following an oxidation modelling approach, Pet. Sci. Technol. 34 (21) (2016) 1768-1776.

[25] G.L. Liu, C.J. Glover, A study on the oxidation kinetics of warm mix asphalt, Chem. Eng. J. 280 (2015) 115-120.

[26] P.R. Herrington, Oxidation of bitumen in the presence of a constant concentration of oxygen, Pet. Sci. Technol. 16 (7-8) (1998) 743-765.

[27] X. Jin, R. Han, Y. Cui, C.J. Glover, Fast-rate-constant-rate oxidation kinetics model for asphalt binders, Ind. Eng. Chem. Res. 50 (23) (2011) 13373-13379.

[28] X. Luo, F. Gu, R.L. Lytton, Kinetics-based aging prediction of asphalt mixtures using field deflection data, Int. J. Pavement Eng. 20 (3) (2019) 287-297.

[29] X. Luo, F. Gu, R.L. Lytton, Prediction of field aging gradient in asphalt pavements, Transp. Res. Rec. 2507 (1) (2015) 19-28.

[30] X. Luo, F. Gu, Y. Zhang, R.L. Lytton, B. Birgisson, Kinetics-based aging evaluation of in-service recycled asphalt pavement, J. Cleaner Prod. 200 (2018) 934-944.

[31] F. Liu, Z. Zhou, Y. Wang, Predict the rheological properties of aged asphalt binders using a universal kinetic model, Constr. Build. Mater. 195 (2019) 283-291.

[32] F. Liu, Z. Zhou, X. Zhang, Y. Wang, On the linking of the rheological properties of asphalt

binders exposed to oven aging and PAV aging, Int. J. Pavement Eng. (2019) 1-10.
[33] X. Luo, F.Q. Ma, Bjorn Birgisson, Z.Y. Huang, Coupled mechanical and kinetic modeling of recovery in asphalt mixtures,Constr. Build. Mater. 254 (2020) 118889.
[34] X. Luo, B. Birgisson, R. L. Lytton, Kinetics of healing of asphalt mixtures, J. Cleaner Prod. 252 (2020) 119790.
[35] H. Li, X. Luo, Y.Q. Zhang, A kinetics-based model of fatigue crack growth rate in bituminous material, Int. J. Fatigue, 148(1) (2020) 106185.
[36] H. Li, X. Luo, W.Z. Yan, Y.Q. Zhang, Energy-based mechanistic approach for crack growth characterization of asphalt binder, Mech. Mater. 148(1) (2020) 103462.
[37] H. Li, X. Luo, Y.Q. Zhang, Pseudo energy-based kinetic characterization of fatigue in asphalt binders, China Journal of Highway and Transport, 33 (10) (2020) 115-124. (in Chinese)
[38] C.Z. Fang, N.S. Guo, Y.Z. Sun, et al., Research on fatigue life of rubber asphalt mixture based on stiffness modulus analysis, Eng. Mech. 36 (1) (2019) 1-10. (in Chinese)
[39] C.Z. Fang, N.S Guo, ZP. You, Y.Q. Tan , et al., Fatigue damage characteristics for rubber asphalt mixture based on energy dissipation history, Journal of Southeast University (Natural Science Edition). (2021). (in Chinese)
[40] Y.Z. Sun, C.Z. Fang, J.C. Wang, et al., Method of fatigue life prediction for rubber asphalt mixture based on plateau value of dissipated energy ratio, J. Build. Materials. 22 (1) (2019) 108-112. (in Chinese)
[41] C.H. Wang, M.H. Wang, Q. Chen, et al., Basic performance and asphalt smoke absorption effect of environment-friendly asphalt to improve pavement construction environment, J. Cleaner. Prod. 2022 (333): 130142.
[42] G. Lu, Z. Wang, P. Liu , et al., Investigation of the hydraulic properties of pervious pavement mixtures: characterization of Darcy and non-Darcy flow based on pore microstructures, Journal of Transportation Engineering, Part B: Pavements, 146(2) (2020) 04020012.
[43] G. Lu, P. Liu, T. Törzs, et al., Numerical analysis for the influence of saturation on the base course of permeable pavement with a novel polyurethane binder, Construction and Building Materials, 240 (2020) 117930.
[44] R. Li, Z. Leng, J. Yang, G. Lu, et al., Innovative application of waste polyethylene terephthalate (PET) derived additive as an antistripping agent for asphalt mixture: Experimental investigation and molecular dynamics simulation, Fuel, 300 (2021) 121015.